Icarus 233 (2014) 306–315

Contents lists available at ScienceDirect

Icarus

journal homepage: www.elsevier.com/locate/icarus

Aromatic and aliphatic organic materials on Iapetus: Analysis of Cassini VIMS data

Dale P. Cruikshank [a,*], Cristina M. Dalle Ore [a,b], Roger N. Clark [c], Yvonne J. Pendleton [a]

[a] NASA Ames Research Center, Moffett Field, CA 94035, United States
[b] SETI Institute, Mountain View, CA 94043, United States
[c] U.S. Geological Survey, Denver, CO 80225, United States

ARTICLE INFO

Article history:
Received 3 December 2013
Revised 7 February 2014
Accepted 8 February 2014
Available online 19 February 2014

We dedicate this paper to the memory of our friend and colleague Dr. Bishun Narain Khare (1933–2013), a pioneer in the study of organic material in planetary atmospheres, on planetary surfaces, and in interstellar space.

Keywords:
Iapetus
Organic chemistry
Satellites, composition
Saturn, satellites

ABSTRACT

We present a quantitative analysis of the hydrocarbon and other organic molecular inventory as a component of the low-albedo material of Saturn's satellite Iapetus, based on a revision of the calibration of the Cassini VIMS instrument. Our study uses hyperspectral data from a mosaic of Iapetus' surface (Pinilla-Alonso, N., Roush, T.L., Marzo, G.A., Cruikshank, D.P., Dalle Ore, C.M. [2011]. Icarus 215, 75–82) constructed from VIMS data on a close fly-by of the satellite. We extracted 2235 individual spectra of the low-albedo regions, and with a clustering analysis tool (Dalle Ore, C.M., Cruikshank, D.P., Clark, R.N. [2012]. Icarus 221, 735–743), separated them into two spectrally distinct groups, one concentrated on the leading hemisphere of Iapetus, and the other group on the trailing. This distribution is broadly consistent with that found from Cassini ISS data analyzed by Denk et al. (Denk, T. et al. [2010]. Science 327, 435–439). We modeled the average spectra of the two geographic regions using the materials and techniques described by Clark et al. (Clark, R.N., Cruikshank, D.P., Jaumann, R., Brown, R.H., Stephan, K., Dalle Ore, C.M., Livio, K.E., Pearson, N., Curchin, J.M., Hoefen, T.M., Buratti, B.J., Filacchione, G., Baines, K.H., Nicholson, P.D. [2012]. Icarus 218, 831–860), and after dividing the Iapetus spectrum by the model for each case, we extracted the resulting spectra in the interval 2.7–4.0 μm for analysis of the organic molecular bands. The spectra reveal the C—H stretching modes of aromatic hydrocarbons at ~3.28 μm (~3050 cm^{-1}), plus four blended bands of aliphatic —CH_2— and —CH_3 in the range ~3.36–3.52 μm (~2980–2840 cm^{-1}). In these data, the aromatic band, probably indicating the presence of polycyclic aromatic hydrocarbons (PAH), is unusually strong in comparison to the aliphatic bands, as was found for Hyperion (Dalton, J.B., Cruikshank, D.P., Clark, R.N. [2012]. Icarus 220, 752–776; Dalle Ore, C.M., Cruikshank, D.P., Clark, R.N. [2012], op. cit.) and Phoebe (Dalle Ore, C.M., Cruikshank, D.P., Clark, R.N. [2012], op. cit.). Our Gaussian decomposition of the organic band region suggests the presence of molecular bands in addition to those noted above, specifically bands attributable to cycloalkanes, olefinic compounds, CH_3OH, and N-substituted PAHs, as well as possible H_n-PAHs (PAHs with excess peripheral H atoms). In a minimalist interpretation of the Gaussian band fitting, we find the ratio of aromatic CH to aliphatic CH_2 + CH_3 functional groups for both the leading and trailing hemispheres of Iapetus is ~10, with no clear difference between them. In the aliphatic component of the surface material, the ratio CH_2/CH_3 is 4.0 on the leading hemisphere and 3.0 on the trailing; both values are higher than those found in interstellar dust and other Solar System materials and the difference between the two hemispheres may be statistically significant. The superficial layer of low-albedo material on Iapetus originated in the interior of Phoebe and is being transported to and deposited on Iapetus (and Hyperion) in the current epoch via the Phoebe dust ring (Tosi, F., Turrini, D., Coradini, A., Filacchione, G., and the VIMS Team [2010]. Mon. Not. R. Astron. Soc. 403, 1113–1130; Tamayo, D., Burns, J.A., Hamilton, D.P., Hedman, M.M. [2011]. Icarus 215, 260–278). The PAHs on Iapetus exist in a H_2O-rich environment, and consequently are subject to UV destruction by hydrogenation on short time-scales. The occurrence of this material is therefore consistent with the assertion that the deposition of the PAH-bearing dust is occurring at the present time. If the organic inventory we observe represents the interior composition of Phoebe, we may be sampling the original material from a region of the solar nebula beyond Neptune where Phoebe formed prior to its capture by Saturn (Johnson, T.V., Lunine, J.I. [2005]. Nature 435, 69–71).
Published by Elsevier Inc.

* Corresponding author.
E-mail address: dale.p.cruikshank@nasa.gov (D.P. Cruikshank).

http://dx.doi.org/10.1016/j.icarus.2014.02.011
0019-1035/Published by Elsevier Inc.

1. Introduction

The presence of aromatic and aliphatic organic materials on the surfaces of Saturn's satellites Phoebe, Iapetus, and Hyperion has been established in previous studies (Clark et al., 2005, 2008, 2012; Cruikshank et al., 2007, 2008; Coradini et al., 2008; Dalton et al., 2012; Dalle Ore et al., 2012) reporting analyses of reflectance spectra of these bodies obtained with the Visible and Infrared Mapping Spectrometer (VIMS) aboard the Cassini spacecraft (Brown et al., 2004, 2006). The identification of these broad classes of organic solid molecular materials is based on the detection of absorption bands characteristic of the C—H stretching modes; in the aromatic material the C—H band complex occurs at ~3.28 μm (~3050 cm^{-1}), and in the aliphatics the most prominent features are four overlapping bands of —CH_2— and —CH_3 in the range ~3.36–3.52 μm (~2980–2840 cm^{-1}) (e.g., Ristein et al., 1998; Matrajt et al., 2005).

The VIMS data for Iapetus were obtained with a spectral sampling interval of 16.7 nm, and the effective spectral resolution is therefore low in comparison with the intrinsic band widths of the spectral features under study (~5–36 nm). In addition, the spectral region in which these bands occur is heavily absorbed by H_2O ice, imposing a steep slope and some possible H_2O ice band structure that must be removed before a quantitative analysis of the organic bands can be made. These factors, plus the low-to-medium signal precision achieved during the brief observing periods as the Cassini spacecraft passed over the satellite surface, add to the challenge of extracting the spectral features of the organic components for comparison of the three bodies with one another, with other astronomical bodies, and with other Solar System materials in a quantitative way.

Cruikshank et al. (2008) noted the unusually strong aromatic band relative to the aliphatic bands in the spectrum of the low-albedo material on Iapetus, and Dalton et al. (2012) found a similar signature on Hyperion. In the present paper we evaluate quantitatively the ratio of aromatic to aliphatic hydrocarbons on Iapetus, and enlarge on the discussion of the possible origin of this apparently unique signature among Solar System solid bodies studied so far.

Dalle Ore et al. (2012) extracted the spectral signatures of the C—H absorption bands in VIMS data for Phoebe, Iapetus, and Hyperion, using mosaics of VIMS image cubes for portions of the satellite surfaces observed at relatively close range during satellite flybys. In particular, a map of the hydrocarbon bands on Iapetus covers portions of both leading and trailing hemispheres. The principal results of that investigation are that (1) the aromatic and aliphatic hydrocarbon bands on all three satellites are confirmed, and as such provide a probable compositional link among these bodies, (2) the aromatic band at 3.28 μm is particularly strong relative to the aliphatic bands, (3) the organic signatures on Iapetus occur in the low-albedo material on both the leading and trailing hemispheres, but there are differences between the leading and trailing signatures that may be attributable to multiple sources (in addition to Phoebe), and (4) the band signatures are uniformly distributed on Hyperion and not especially concentrated in the low-albedo material, as Dalton et al. (2012) had noted. Dalle Ore et al. (2012) concluded that material migrating from the dust ring filling Phoebe's orbit (Verbiscer et al., 2009) can be traced to Iapetus and to Hyperion through the similarity in the organic spectral signature. They also concluded that differences in the signature on the leading and trailing hemispheres of Iapetus are suggestive of dust from two different sources, one of which predated the current epoch of Phoebe dust deposition. A surface compositional link among these three satellites had been suggested earlier by Jarvis et al. (2000). Below we consider this issue further.

Since the publication of the Dalle Ore et al. (2012) paper, we learned that a correction to the derived spectra of all three satellites must be made because of an ambiguity in the radiometric calibration applied to VIMS data in the pipeline calibration procedure. Although Dalle Ore et al. (2012) noted that their data were reduced using the pipeline RC-17 calibration,[1] in fact those data used the earlier RC-15 calibration; the error occurred in the VIMS data base and was discovered only after the publication of Dalle Ore et al. (2012). The correction we use in the present paper, which is incorporated in the VIMS calibration designated RC-17, is especially important in the spectral interval ~2.9–3.4 μm, the region that includes the aromatic CH band and the shortest wavelength components of the aliphatic CH band complex. Accordingly, we have reduced and reanalyzed the Iapetus data set used in the Dalle Ore et al. (2012) analysis. As described below, we extracted the organic band signatures from the data (3.0–3.7 μm) by a different technique that depends on an accurate model of the spectrum and thereby allows for a reliable removal of the signature of H_2O ice in the organic band region.

2. The VIMS data

The process of extracting the organic spectral bands from the VIMS data set begins with a clustering analysis performed on the spatially resampled mosaic of VIMS image cubes described by Pinilla-Alonso et al. (2011, their Fig. 1). The data were obtained on the Iapetus flyby of September 10, 2007, when the range of the Cassini spacecraft to Iapetus varied from about 2400 to 5000 km, and the phase angle varied from ~13° to 100°. The clustering algorithm is described by Pinilla-Alonso et al. (2011) and Dalle Ore et al. (2012); for the present analysis the wavelength interval over which the cluster analysis classified each spatial pixel in the mosaic was 2.9–3.8 μm. This wavelength interval is particularly sensitive to the abundance of H_2O ice. The cluster that showed minimum ice absorption and the lowest albedo was selected for further analysis. Each spatial pixel in that cluster was individually fit with a polynomial spline, using as tie points the same wavelengths used in the analysis by Dalle Ore et al. (2012): 3.007, 3.090, 3.190, 3.200, 3.345, 3.529, 3.530, 3.612, 3.640, and 3.659 μm. After dividing each pixel by the spline fit and running the clustering algorithm again, the Iapetus data set clearly divided into a primarily leading hemisphere and a trailing hemisphere group. The cluster for the leading hemisphere contains 1329 spatial pixels, and that for the trailing hemisphere 906 pixels. There were a small number of dark, ice-poor pixels that fell at other locations in the mosaic, but these are ignored in the subsequent analysis.

We note that the problem of removing the strong background absorption of ice for the extraction of the organic bands is analogous to that encountered in the study of aliphatic hydrocarbon spectral features in the interstellar medium (e.g., Sandford et al., 1991; Pendleton et al., 1994; Dartois et al., 2004a). In those studies it was found that differences in continuum baseline selections might result in slight changes to absolute values of the calculated abundances of the CH_2 and CH_3 functional groups in the aliphatic molecular components of the dust, but the relative strengths of the CH_2 to CH_3 bands remained constant and the ratio CH_2/CH_3 was robust.

Using the average spectra computed for each of the two clusters identified above, we calculated Hapke models for the original data before the spline fitting. The models consist of H_2O ice at temper-

[1] The RC-17 calibration is part of the VIMS data processing pipeline at the VIMS Operations Center, Lunar and Planetary Lab., University of Arizona. VIMS data processed since approximately December 1, 2012, utilize the RC-17 calibration file.

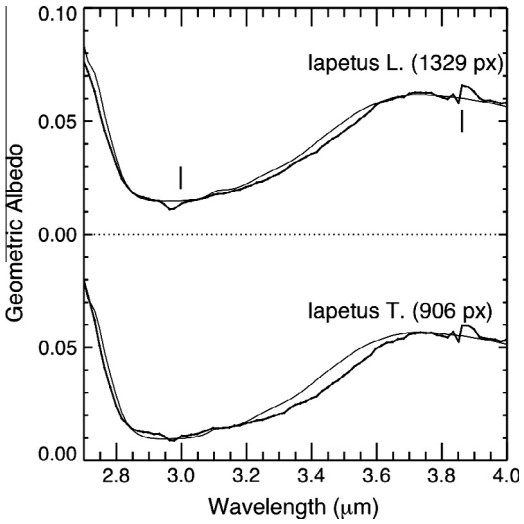

Fig. 1. Best-fitting Hapke models (thin lines) for the 2.7–4.0-μm region of the spectra of the selected spatial pixels (px) for the low-albedo material on the leading (L) hemisphere of Iapetus. The same model, with a vertical offset of −0.005 is applied to the trailing (T) hemisphere spectrum. Model details are given in Appendix A. Two vertical dashes in upper panel indicate wavelengths with artefacts introduced by VIMS filter junctions. The noise value for each spectrum is described in the caption to Fig. 2.

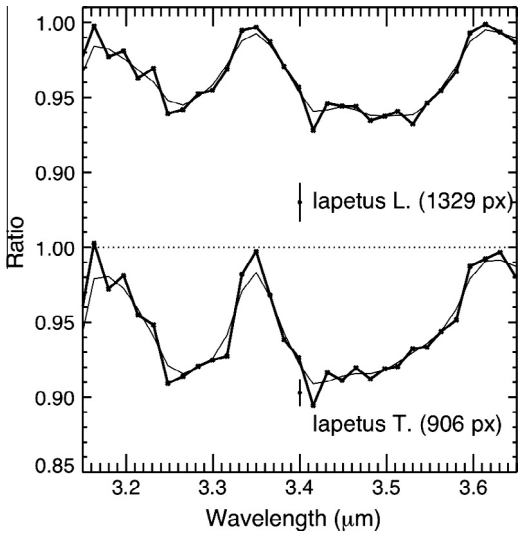

Fig. 2. Comparison of Iapetus leading (L) and trailing (T) dark material signatures. The average sampling interval of the original data is 16.7 nm. Statistical errors in each spectrum were evaluated by flattening the spectra and measuring the standard deviation, as described in Cruikshank et al. (2008). In the units shown on the ordinate, the results are: Iapetus trailing $\sigma = 0.013$, Iapetus leading $\sigma = 0.009$; a representative error bar is shown for each spectrum.

ature $T = 120$ K (see Appendix A) as shown in Fig. 1. The Iapetus data in each cluster were then divided by the best-fit model to give the residual spectra shown in Fig. 2.

3. Analysis

Having established the presence of spectral signatures of aliphatic and aromatic molecules on the surface of Iapetus, we can proceed toward a quantitative analysis with the goals of determining the relative abundances of —CH_3 and —CH_2— functional groups and the ratio of CH groups in aromatic and aliphatic molecules. Regrettably, the identification of specific molecules of refractory organic materials in the solid state is not possible using remote sensing techniques with this spectral resolution and range.

Furthermore, the unknown penetration depth of solar photons into the surface of a solid planetary body and then scattered back to space where they are detected thwarts the calculation of reliable abundances (column densities). Cruikshank et al. (2008) roughly estimated that for an optical penetration depth of 100 μm into surface material having density 1 g/cm^3 and mean molar mass 300 g/mole (small organic molecules), the Iapetus spectrum yields a range of 10^{-4} to 10^{-3} g/cm^3 of aromatic molecules. In this simple calculation, the penetration depth is the least reliable quantity.

3.1. Aliphatic hydrocarbon: CH_2 and CH_3 groups

Although we cannot detect specific molecules or calculate abundances reliably in the VIMS Iapetus data, we can estimate the relative amounts of —CH_2— and —CH_3 groups in the aliphatic components and the relative amounts of CH groups in the aromatic and aliphatic components. In the first case, the ratio of —CH_2— to —CH_3 groups is a measure of the sizes of the chain-like aliphatic molecular structures because they occur in the middle and the ends of the chains, respectively. The relevance of this ratio is that thermal and radiation processing of long-chain aliphatics tends to break the chains and allow the molecular fragments to recombine into more compact structures, with the loss or redistribution of H atoms. Even relatively short-chain alkanes and alkenes are affected by irradiation; Hand and Carlson (2012) found that electron irradiation of ice mixtures of H_2O with three alkanes and three alkenes resulted in the formation of —OH and C=O bonds and the formyl radical. Polymeric residues from the irradiation had $CH_2/CH_3 \sim 1.5$. Thus, small values of CH_2 relative to CH_3 can be a measure of the degree of processing or aging of material on a planetary surface. [Henceforth, we denote the two groups as CH_2 and CH_3 without the valence notation.] The situation can be much more complex, however, because of branching along the aliphatic chain, in which CH_3 and CH_2 functional groups can appear at various places, thus affecting the CH_2:CH_3 ratio, depending on which groups are preferentially added.

The spectral interval ~3.23–3.55 μm (3096–2817 cm^{-1}) is the site of several modes of absorption (and emission) in organic compounds., including both the symmetric and asymmetric modes of both CH_2 and CH_3, CH in cycloalkanes (Silverstein et al., 1981), as well as olefinic CH and CH_2 (olefins have at least one double-bonded C atom pair, as in —C=C—). Furthermore, there are tertiary CH groups that absorb near 2890 cm^{-1} (3.460 μm), but this band is normally weak (Silverstein et al., 1981). Other factors that affect the frequency of the characteristic C—H stretching modes involve interactions with lone pair electrons in groups containing N and O in an aliphatic chain (Bellamy, 1975). This lone pair interaction can cause a significant frequency change in CH_3 to as low as 2775 cm^{-1} (3.617 μm), and similar effects occur with CH_2 frequencies. These bands are listed in Table 1, although this is not an exhaustive compilation.

Among the standard four aliphatic bands, the asymmetric modes of CH_2 and CH_3 are the strongest components of the band complex, and the symmetric modes of CH_2 and CH_3 are next in strength. As noted, the tertiary CH tends to be weak, and the olefinic bands are negligibly weak in astronomical sources. We also include a band at longer wavelength associated with CH_3 in a lone pair with atoms in nitrogen or oxygen groups (Bellamy, 1975), again because of apparent absorption in the Iapetus spectra and because this is a plausible molecular configuration in the surface inventory of the satellite.

We have included in Table 1 the υ_3 band in CH_3OH ice at 2827 cm^{-1} (3.537 μm) because it and a broader methanol complex (υ_2 at 3.349 μm and υ_9 at ~3.384 μm) are possible components of

Table 1
Functional groups exhibiting absorption bands in the spectral region considered in this paper.

Assignment	Freq (cm^{-1})	Wavelength (μm)	FWHM (cm^{-1})
Cycloalkane CH[a]	*3098*	*3.228*	*30*
Olefinic CH_2 (asymmetric)[b]	*3078*	*3.248*	*~26*
Olefinic CH[b]	*3010*	*3.326*	*~50*
Olefinic CH_2 (symmetric)[b]	*2985*	*3.350*	*~20*
Aliphatic —CH_3 (asymmetric)[b]	2958	3.381	28.2
Aliphatic —CH_2— (asymmetric)[b]	2926	3.418	27.5
Tertiary CH[a]	*2890*	*3.460*	
Aliphatic —CH_3 (symmetric)[b]	2871	3.483	25.6
Aliphatic —CH_2— (symmetric)[b]	2850	3.509	34.9
CH_3OH ice[c]	*2827*	*3.537*	30
CH_3 + lone pair in N, O[d]	*2830–2765*	*3.534–3.617*	

[a] Silverstein et al. (1981).
[b] Band frequencies (wavelengths) and FWHM (full width at half-maximum intensity) are the averages for three laboratory samples from Dartois et al. (2004b).
[c] CH_3OH has additional bands at slightly shorter wavelengths; e.g., Cruikshank et al. (1998) and d'Hendecourt and Allamandola (1986).
[d] Bellamy (1975) (p. 17). For entries in italics, see below.

the excess absorption in the Iapetus spectra that is not accounted for by the basic aliphatic CH_2 and CH_3 bands. The υ_3 band is observed in most comet comae (e.g., Bockelée-Morvan et al., 1995; Mumma and Charnley, 2011). Solid methanol is found on other Solar System bodies; the 2.27-μm combination band, which is intrinsically much weaker than υ_3, is present on Centaur object 5145 Pholus (Cruikshank et al., 1998) and the transneptunian object 55638 (2002 VE_{95}) (Barucci et al., 2006). We note that weak absorption features in the spectra of the low-albedo material on Iapetus in the region 2.1–2.4 μm where H_2O ice absorption is minimal are consistent with the presence of the 2.27-μm CH_3OH band (see Figs. 3a, 3c, 15 of Clark et al., 2012). The possible occurrence of CH_3OH on Iapetus will be the subject of a subsequent paper.

A further potential source of absorption in the aliphatic region, not listed in Table 1, arises from small H_n-PAHs, which are polycyclic aromatic hydrocarbons that have excess hydrogen on the periphery, or from PAHs with attached CH_3 groups. Bernstein et al. (1996) and Sandford et al. (2013) have presented laboratory spectra of several H_n-PAHs with various degrees of H addition. The basic spectral pattern of addition of successive H atoms on the aromatic rings is that the simple aromatic CH band gains complexity and shifts a small amount in wavelength, while CH_2 bands in the aliphatic region grow and shift in wavelength, with some as long as 3.556 μm (2812 cm^{-1}). With the multiplicity of bands produced in the aliphatic spectral region as peripheral H is added to the aromatic rings, it seems clear that these bands, together with the basic CH_2 and CH_3 (symmetric and asymmetric) modes, can fill a large envelope of absorption such as we see in the spectrum of Iapetus under study here. Hydrogenation of PAHs readily occurs at 100 K when PAHs in H_2O ice are UV-irradiated (Bernstein et al., 1996; Gudipati and Yang, 2012). In the surface environment at Iapetus, with the availability of H_2O and the solar UV flux, exposed PAHs will be hydrogenated *in situ* on relatively rapid timescales.

3.2. Aromatic hydrocarbons: CH groups

Aromatic hydrocarbons have a characteristic CH stretching mode band of often complex structure that is typically centered near 3.28 μm. This band characteristically consists of two or three closely adjacent components, the positions and widths of which, as noted by laboratory measurements (e.g., Colangeli et al., 1992; Hudgins and Sandford, 1998) and theoretical calculations (e.g., Bauschlicher et al., 2008) vary over the range ~3118–3032 cm^{-1} (3.207–3.298 μm). Several factors affect the precise position of the 3.28-μm band in PAHs (e.g., Allamandola, 2011), including charge state, molecular heterogeneity and molecule size, with the charge state as the principal determinant of the central frequency of the band. Laboratory studies of isolated PAHs of many sizes in the neutral, anionic, and cationic charge states show that the band center for PAH anions occurs in the range 3085–3025 cm^{-1} (3.241–3.306 μm), neutral PAHs in the range 3094–3042 cm^{-1} (3.232–3.287 μm), and PAH cations in the range 3112–3073 cm^{-1} (3.213–3.254 μm). The central frequencies for PAH anions, large neutrals (number of C atoms $\geqslant$40), small neutrals (number of C atoms <40), and cations are 3048, 3081, 3063 and 3093 cm^{-1} (3.281, 3.246, 3.265 and 3.233 μm, respectively) (van Diedenhoven et al., 2004).

We include in the aromatic inventory a CH band observed in pyridine extracts from coal (Sobkowiak and Painter, 1992). Pyridine (C_5H_5N) is related to a benzene ring, but with one N-atom substituted for a C-atom in the ring. This infrared-active band (Corrsin et al., 1953) at 3017 cm^{-1} (3.314 μm) is included because it contains a nitrogen atom, consistent with the appearance of lone-pair bands probably related to N and O in the aliphatic region (see above). In addition, it absorbs at a lower frequency than the CH bands in PAHs (neutral and ionized) where our Iapetus spectra show absorption.

The band widths adopted in the Bauschlicher et al. (2008, 2009) and Ricca et al. (2012) papers are a uniform 30 cm^{-1}, selected because of the general appearance of the bands when seen in emission (Wagner et al., 2000). In the theoretical calculations the band intensities are integrated over the computed band envelope, and do not depend on the choice of band width for the calculations (C. Bauschlicher, private communication, 2013). Band widths of PAHs observed in absorption (in matrix isolation) in the laboratory are variable, and characteristically ~25–50 cm^{-1} (e.g., Hudgins and Sandford, 1998; Sandford et al., 2013). When organic ices are observed in diffuse reflectance, the bands are commonly 30–50% broader than the corresponding bands seen in absorption (Clark et al., 2009), but in the analysis presented here, we consider two basic aromatic bands of width 30 cm^{-1} each and of equal intrinsic strength (*A*-value), as shown in Table 2. In terms of calculating relative abundances of aromatic and aliphatic CH bonds (Section 3.4), this is a conservative approach; the actual aromatic CH may be substantially greater.

It is also important to note that the aromatic molecules revealed by their peripheral CH or CH_n bands can be arbitrarily large, because in the wavelength region available in this study only those peripheral bonds with hydrogen produce detectable spectral bands. Thus, the total molecular mass of aromatics can be large, as is found to be the case with some PAH-bearing materials such as interplanetary dust particles, comet samples returned by the *Stardust* mission, carbonaceous meteorites, and micrometeorites

Table 2
Functional groups exhibiting absorption bands in the aromatic spectral region considered in this paper.

Assignment	Freq (cm^{-1})	Wavelength (μm)	FWHM (cm^{-1})
Aromatic CH[a]	3067	3.260	30
Aromatic CH[a]	3049	3.280	30
Aromatic CH (pyridine)[b]	3017	3.314	30

[a] The frequencies/wavelengths are for the CH stretching mode in neutral polycyclic aromatic hydrocarbons (PAH), averaged over a number of molecules for which theoretical calculations have been made (Bauschlicher et al., 2008, 2009; Ricca et al., 2012). The full-width half-maximum (FWHM) values were adopted for the calculations in the Bauschlicher et al. and Ricca et al. papers; see text.

[b] CH in pyridine (C_5H_5N) observed in pyridine extracts from coal (Sobkowiak and Painter, 1992).

investigated in the laboratory (e.g., Sandford, 2008; Clemett et al., 1998, 2010; Flynn et al., 2004). Fig. 17 of Pendleton and Allamandola (2002) illustrates this point; large aromatic sheets can contain a large mass of carbon, while only the H-atoms and aliphatic units on the edges of the sheet are spectrally active. Similarly, in the wavelength region in which we can observe Iapetus, it is possible that large amounts of carbon escape detection.

3.3. Gaussian band fitting

For the derived spectra of the low-albedo material on both the leading and trailing hemispheres of Iapetus (Fig. 3A and C), we have fit Gaussians defined in wavelength and band width to correspond to (1) two aromatic bands found in the laboratory and in theoretical computations, and (2) the four "basic" aliphatic bands attributed to the asymmetric and symmetric modes of CH_2 and CH_3 similarly derived from the laboratory and calculations. Although these six bands do not fill the absorption area of either spectrum of Iapetus, the band intensities (in optical thickness) derived from this fit can be compared with similar fits to spectra of other extraterrestrial materials.

In Fig. 3A, C and B, D we shows the results of a Gaussian band fit to the same Iapetus spectra using all of the bands in Tables 1 and 2, respectively. It is clear in Fig. 3A and C that the plotted Gaussian do not fill the absorption areas in either the aromatic or aliphatic spectral intervals. If we try to account for the additional absorption by including additional plausible bands with a typical FWHM width of ~30 cm^{-1}, we find that the absorption envelope can be approximately filled. The inclusion of these additional bands does not constitute the identification of the specific modes listed in Tables 1 and 2, but is instead a notional view of the variety of modes that may be contributing to the overall observed absorption. The bands considered notional are shown in italics in Tables 1 and 2. For completeness we show in Tables A1 and A1 (Appendix) the derived bandwidths and optical depths from the Gaussians fit to the absorption envelope in Fig. 3B and D.

Calculation of the ratio of CH groups in aromatic and aliphatic molecules from the spectrum requires a measurement of the band strengths in the data plus knowledge of the absolute strengths (*A*-values) of the bands or band components per molecule (the proportionality coefficients for the energies of the stretching modes in the molecule). The absolute strengths of stretching modes have been measured by several investigators (e.g., references in Wexler, 1967; Matrajt et al., 2005), and scaled (to laboratory measurements) from molecular theory for a number of polycyclic aromatic

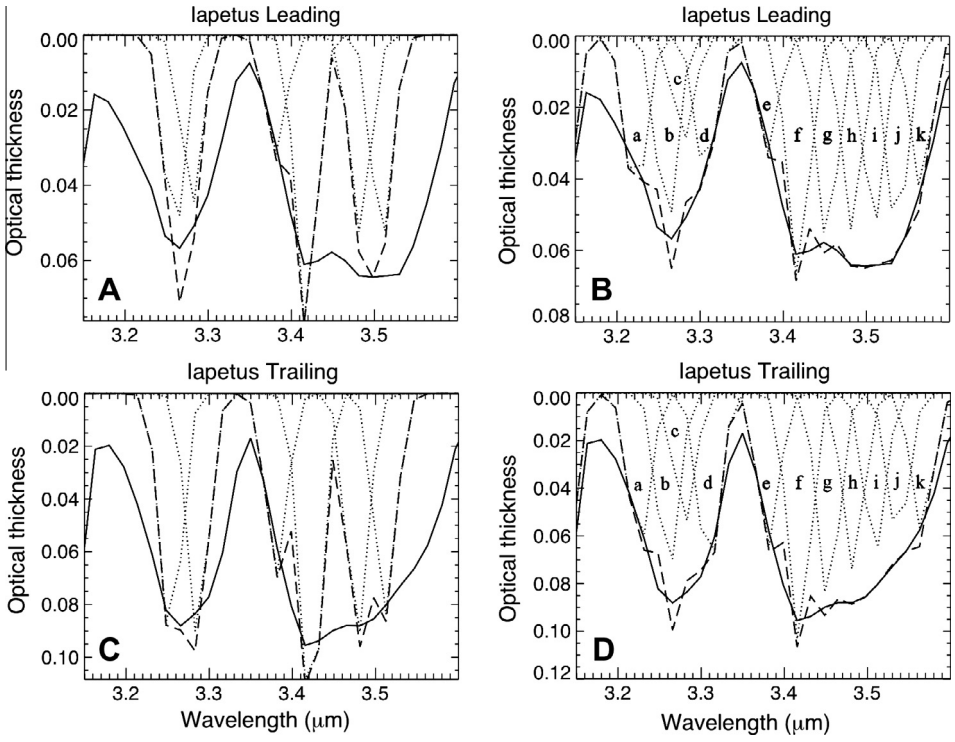

Fig. 3. Gaussian band fits to the absorption spectra of the leading (panels A and B) and trailing (panels C and D) hemispheres of Iapetus. The original extracted spectrum for each hemisphere is shown in Fig. 1. In the versions shown here (solid lines) the spectra are smoothed (with a five-point Gaussian) so that the MGM (Modified Gaussian Method of Sunshine et al., 1989) routine can reach convergence. The dotted lines are the Gaussians found by the fitting software and the dashed lines show the sum of those Gaussians in each panel. Panels A and C show the fit with only two bands in the aromatic region and the four basic bands in the aliphatic region (see Tables 1 and 2). Panels B and D show a full set of Gaussians that includes the wavelengths and characteristics of the basic bands, plus other molecules and functional groups that are plausible components of the low-albedo material on Iapetus; the lower-case letters refer to the specific bands in Tables A1 and A2. See Tables 1 and 2 for band identifications in panels A and C and text for discussion.

hydrocarbons (PAHs) (Bauschlicher et al., 2008, 2009; Ricca et al., 2012).

In the quantitative analysis of the organic bands in the Saturn satellite spectra, we encounter the limitations imposed by low spectral resolution (sampling interval ~14 cm^{-1} at 3.4 μm), as well as the common problem of low signal precision. Also, the process of extraction of the organic absorption bands from the steep continuum absorption introduces an additional uncertainty in the band intensity relative to the reconstructed, or artificial, continuum level. The band ratios, however, are expected to be robust despite the uncertainty in setting the continuum level.

The intrinsic half-widths of the two strongest aliphatic bands are of order 30 cm^{-1}, and the ideal spectral resolution to give a clear indication of the band profiles and their correct intensities is about 4 cm^{-1} (Wexler, 1967), or about four times higher than the VIMS spectral sampling interval quoted above. In a well resolved spectrum, the four CH_2 and CH_3 bands partially overlap, and each component can be approximated by a symmetric Voigt profile. The consequence of the low VIMS resolution is that the intensities of the most prominent asymmetric CH_2 and CH_3 bands are underestimated. However, since all of the band components we are fitting have intrinsic widths of ~30 cm^{-1} and we are using approximately the same width for each of the Gaussian bands in our fitting procedure, all of the intensities should be systematically underestimated by about the same amount, and thus the band ratios we calculate should be relatively unaffected.

In order to measure the strengths of the aromatic and aliphatic absorption bands in the two average spectra we are using for the low-albedo material on Iapetus (one cluster geographically selected on the leading hemisphere and the other on the trailing hemisphere), we used the modified Gaussian model (MGM) of Sunshine et al. (1989) and Sunshine and Pieters (1993). We took two approaches to the Gaussian fitting. In both sets of calculations, we specified the same two band centers and band widths for the aromatic component, and in one set of calculations we specified the band centers and band widths for four aliphatic components. In the second set of calculations, we specified the band widths for four aliphatic components, but let the fitting routine find the preferred band centers. In all cases, the MGM calculations found slightly different band widths than we specified, which were 30 cm^{-1} in all instances for both aromatic and aliphatic bands. The results of the calculations are shown in Tables 3 and 4, for the leading and trailing hemisphere spectrum clusters, respectively.

Using only the minimum fitting of Gaussians to the Iapetus data (two in the aromatic region, four in the aliphatic region), we derive the number of CH groups for each band.

To calculate the number, *N*, of CH bonds in the aromatic molecular components, for each of the bands considered separately, we use the approximation by d'Hendecourt and Allamandola (1986).

$$N_c = \tau_v v / A,$$

where τ_v is the optical depth of the band, v the width of the band (in cm^{-1}), and A is the absolute strength of a molecular spectral band (cm/CH group).

3.4. Ratio of aromatic CH to aliphatic CH

Using the calculated values of *N* for the two aromatic CH bands added together and the sum of the values of *N* for the asymmetric aliphatic bands (a-CH_2 and a-CH_3), we calculate the ratio of CH *groups* in these components, and find that for the leading hemisphere $(\text{aromatic/aliphatic})_L \sim 9$. The same calculation for the trailing hemisphere is $(\text{aromatic/aliphatic})_T \sim 10$; these two values do not appear to be significantly different from one another. Since CH_2 has two CH bonds and CH_3 has three, we can make the comparison in terms of the total number of CH *bonds*. This calculation results in $(\text{aromatic/aliphatic})_L = 4.1$, and $(\text{aromatic/aliphatic})_T = 4.4$; the difference in these two values is not considered significant.

3.5. Ratio of CH_2 to CH_3

As noted above (Section 3.1), the relative numbers of CH_2 and CH_3 functional groups in aliphatic molecules are indicative of chain length, which in turn can be related to the origin and processing of simple aliphatic molecules and to the aliphatic components of macromolecular organic materials. From the calculations shown in Tables 3 and 4, for the leading hemisphere of Iapetus, $(CH_2/CH_3)_L = 4.0$, while for the trailing hemisphere it is $(CH_2/CH_3)_T = 3.0$. The difference in these two values, for which we estimate the statistical error to be ±15%, appears to be physically significant. It is seen in Tables 3 and 4 that the numbers (*N*) of CH groups derived for the symmetric modes of CH_2 and CH_3 are large, even though their intrinsic strengths (the *A*-values) are substantially smaller than those for the asymmetric modes. The derived abundances for a-CH_3 and s-CH_3 (and correspondingly for a-CH_2 and s-CH_2) should be the same to within the accuracy of the *A*-values used and the accuracy of the spectral data for the two sides of Iapetus. We attribute the apparent anomalous strength of the symmetric modes to the presence of additional absorption by other molecular modes in the relevant spectral region (~3.45–3.55 μm); see Fig. 3B and D, and Appendix A.2.

For the case of the asymmetric modes, we find the ratios $(\text{a-}CH_2/\text{a-}CH_3)_{LT}$ are notably larger than the ratio found in the dust in the diffuse interstellar medium along several sight lines through the galactic diffuse interstellar medium (ISM) (e.g., Sandford et al., 1991; Pendleton et al., 1994), where the ratio lies in the range 2.0–2.5. The Iapetus values also are larger than those found for interstellar dust in the Seyfert galaxy IRAS 08572+3915 (Wright et al., 1996; Pendleton, 2004) which are closely similar to the diffuse ISM in our Galaxy. In addition, Dartois et al. (2004a) found $CH_2/CH_3 \sim 2$ for a sample of four Seyfert type 2 galactic nuclei. Our result presented here suggests a preponderance of long-chain or highly branched molecular structure in the aliphatic components of the organics on the surface of Iapetus in comparison to interstel-

Table 3
Results for leading hemisphere.

Band identification	Central wavelength (μm)	Derived FWHM of band (cm^{-1})	Optical depth of band, τ	*A*-value (cm per CH group)	N CH groups
Aromatic CH	3.259[1]	30.1	0.054	8.30E−19[3]	2.0E18
Aromatic CH	3.280[1]	30.0	0.045	8.30E−19[3]	1.6E18
Aliphatic a-CH_3	3.381[2]	30.0	0.032	1.20E−17[4]	8.0E16
Aliphatic a-CH_2	3.418[2]	30.2	0.078	7.40E−18[4]	3.2E17
Aliphatic s-CH_3	3.483[2]	30.2	0.053	2.10E−18[4]	7.6E17
Aliphatic s-CH_2	3.509[2]	30.2	0.054	2.10E−18[4]	7.8E17

In this table a-CH_3 and a-CH_2 refer to the asymmetric vibrational modes, while s-CH_3 and s-CH_2 refer to the symmetric modes. Sources of listed values: [1] Bauschlicher et al. (2008), [2] Dartois et al. (2004a), [3] Wexler (1967), [4] Sandford et al. (1991).

Table 4
Results for trailing hemisphere.

Band identification	Central wavelength (μm)	Derived FWHM of band (cm^{-1})	Optical depth of band, τ	*A*-value (cm per CH group)	N CH groups
Aromatic CH	3.254	30.4	0.096	8.30E−19[3]	3.5E18
Aromatic CH	3.286	30.6	0.093	8.30E−19[3]	3.4E18
Aliphatic a-CH_3	3.381	30.3	0.069	1.20E−17[4]	1.7E17
Aliphatic a-CH_2	3.422	31.3	0.124	7.40E−18[4]	5.2E17
Aliphatic s-CH_3	3.478	31.0	0.093	2.10E−18[4]	1.4E18
Aliphatic s-CH_2	3.512	30.7	0.084	2.10E−18[4]	1.2E18

In this table a-CH_3 and a-CH_2 refer to the asymmetric vibrational modes, while s-CH_3 and s-CH_2 refer to the symmetric modes. Sources of listed values: [3] Wexler (1967), [4] Sandford et al. (1991).

lar dust both in the Milky Way and Seyfert galaxies. Longer molecular chains and/or more molecular branching in leading hemisphere aliphatics than those on the trailing hemisphere could indicate greater age of the trailing surface units, since exposure to the space environment tends to destroy longer structures. This in turns would generally support the notion that the organics on the leading hemisphere are younger, a result consistent with the view that they are being emplaced in the current epoch (see Section 4).

4. Discussion

4.1. Characteristics of the spectra

The presence of the aromatic CH band in conjunction with the aliphatic CH stretching modes in the same surface material of a Solar System body is uncommon among the extraterrestrial materials available for laboratory study and among the bodies studied by remote sensing up to the present time. Although interplanetary dust particles (IDP), certain carbonaceous meteorites, and comet particles returned by the *Stardust* mission all have both aromatic and aliphatic molecular components, the spectroscopic appearance of a strong aromatic band at 3.28 μm is rare; the aromatic CH band in nearly all such materials is undetectably small or at best very weak ($\leqslant$0.1) in comparison with the aliphatic band strength (Matrajt et al., 2005, 2013). An exception is the aromatic CH band in the unusual Tagish Lake meteorite (C.M.O'D. Alexander, private communication), in which the aromatic band depth is comparable to the aliphatic maximum band depth.

In polycyclic aromatic structures the hydrogen atoms bond only to the peripheral carbon atoms; the number of such CH bonds that can be detected in the spectrum therefore is not directly indicative of the total amount of aromatic hydrocarbon material in a sample. Other spectral regions (e.g., $6.2 < \lambda < 8.6$ μm) unavailable to us show the C═C stretching mode in polycyclic aromatic hydrocarbons, and therefore are more indicative of the size of the PAH and the degree to which N atoms have substituted for C atoms in the structure (Bauschlicher et al., 2009). Samples of extraterrestrial material studied in the laboratory by various techniques other than near-infrared spectroscopy (Raman spectroscopy, laser desorption mass spectroscopy, nuclear magnetic resonance spectroscopy) also show that interplanetary dust particles, comet dust, carbonaceous meteorites and micrometeorites all contain significant quantities of aromatic hydrocarbons, although the CH bands near 3.0 μm are generally not prominent because the number of C═C bonds is much greater than the peripheral C—H bonds (e.g., Sandford et al., 2006; Sandford, 2008; Clemett et al., 2010).

We noted above that the present analysis is specific to Iapetus and the revised analyses of Hyperion and Phoebe are pending. The results of Dalle Ore et al. (2012) show, however, that similar organic spectral signatures are found on all three satellites. The unusual but similar shared organic spectral signatures show a connection among these bodies. Dalle Ore et al. (2012) suggest that while the current and known active source of dust moving inward and encountering Iapetus' leading hemisphere is the Phoebe ring (Verbiscer et al., 2009), collisional dust from other outer saturnian satellites may account for differences in the material on Hyperion, and possibly for the differences between the trailing and leading hemispheres of Iapetus shown here. This proposal is consistent with the study by Bottke et al. (2010) of collisional grinding among the outer satellites other than Phoebe, and the identification by Denk et al. (2010) of two types of low-albedo material on Iapetus. Tosi et al. (2010) also concluded that there may be multiple sources of the low-albedo material on Iapetus and Hyperion, with contributions from satellites exterior to Phoebe over the lifetime of the Saturn system.

A quantitative analysis of the Hyperion and Phoebe organics will be presented when suitable models of their spectra can be calculated; this work is pending a revision to the Mastrapa et al. (2009) optical constants for H_2O ice at the temperatures relevant to these two satellites.

4.2. Phoebe as the source of the Iapetus organic materials

Material excavated and pulverized from Phoebe by a collision represents Phoebe's bulk properties in terms of organic, ice, and mineral content. Thus, the molecular and optical properties of the excavated material can be different from those of the material lying on the uppermost surface where it is exposed to the space environment. It has long been noted (e.g., Cruikshank et al., 1983) that the color of the integrated disk of Phoebe is different (less red) from that of the low-albedo material of Iapetus; this difference is clearly shown in the thorough study of the color and spectral properties of all the Saturn satellites from VIMS data by Filacchione et al. (2012, their Fig. 1). Most specific to our study here, the color difference has been interpreted as a result of the ion bombardment of Phoebe's surface to a depth of order one millimeter (Strazzulla, 1986). Ion bombardment, simulated in the laboratory by MeV protons, dehydrogenates and carbonizes organic solids, resulting in a neutral gray surface of low albedo on a timescale <10 My for protons with energies 1–2 MeV (Strazzulla, 1986). The deeper levels of Phoebe are subject to processing by >4 Gy exposure to energetic (~GeV) cosmic rays, which can penetrate meters of solid material (Johnson, 1989; Strazzulla et al., 2003). Cosmic ray processing also occurs on comets, which after a similar exposure age show the presence of organic molecules during outgasing, dust ejection, and complete disruption. Whatever long-term molecular processing by cosmic rays may occur in the interior of an icy body in the outer Solar System, a diverse organic inventory (including PAHs) remains to the present epoch. This diversity is seen in particles collected from Comet 81P/Wild 2 (Sandford, 2008).

Another solution to the issue of the difference between Phoebe and Iapetus is independent of the organic content of the surfaces, which in either case may be too low to affect the colors. Clark et al. (2012) modeled VIMS spectra of both bodies over the full

wavelength range (0.35–5.1 μm) and showed that the difference could be simply explained by the nano-phase iron abundance mixed in the ice, with Phoebe having higher concentrations of nano-iron than the dark material on Iapetus. We note also that cosmic ray processing of any iron-bearing silicates present on the surfaces will create nano-phase iron on the surfaces of silicate grains (Carrez et al., 2002).

In terms of the organic materials on Iapetus, the processes of dehydrogenation and carbonization of organic solids by radiation must be reconciled with the UV hydrogenation of PAHs in ice to produce H_n-PAHs (Bernstein et al., 1996; Sandford et al., 2013) mentioned above, and the facile hydrogenation and hydroxylation of PAHs embedded in H_2O ice reported by Gudipati and Yang (2012). Dehydrogenation of PAHs on the surface causes alteration to a graphitic or amorphous carbon state. In contrast, the addition of peripheral hydrogen destroys the aromatic spectral signature at 3.28 μm. Which of these processes dominates on Iapetus, and by implication on Phoebe and Hyperion, is not clear, but the effects of the space environment are in any case unfavorable to the very long-term survival of polycyclic aromatic hydrocarbons and their aromatic spectral signature near 3.3 μm. Under the surface, however, PAHs shielded from solar and galactic UV can persist for astronomical timescales. It therefore follows that the appearance of PAHs on the icy surfaces of Phoebe, Hyperion, and Iapetus indicates recent emplacement, and that the source of the material is from the shielded interior of the parent body (Phoebe). Dust fragments consisting of PAHs in intimate association with H_2O ice recently excavated from the interior Phoebe and precipitating in the current epoch on the surfaces of Phoebe itself, Iapetus, and Hyperion meet these requirements.

5. Conclusions

Saturn's three large satellites exterior to Titan are linked in a compositional sense by a unique spectral signature representative of aromatic and aliphatic hydrocarbons (Clark et al., 2005, 2012; Coradini et al., 2008; Dalton et al., 2012; Dalle Ore et al., 2012). This discovery effectively confirms the long-held assertion that material ejected from Phoebe and possibly other outer satellites has made its way to Iapetus and Hyperion, where it now lies on their surfaces. Together with the hydrocarbon link described here, the detection of the Phoebe ring (Verbiscer et al., 2009), the elucidation of the dynamical mechanism for the transfer of that dust to Iapetus and Hyperion (Tosi et al., 2010; Tamayo et al., 2011), and the potential dust from collisions among other outer satellites (Bottke et al., 2010; Tosi et al., 2010) the entire scenario is brought to a logical conclusion.

The low-albedo material on the leading hemisphere of Iapetus is different in both color (Denk et al., 2010) and near-infrared spectral signature (Clark et al., 2012), including the hydrocarbon band signature (Dalle Ore et al., 2012, this paper). This difference may indicate different sources of the two varieties of the low-albedo material; dust currently precipitating from the Phoebe ring is the favored source for the material on the leading hemisphere of Iapetus. Alternatively, the difference in color can be accounted for by varying abundances of the ice:nano-phase iron ratio and the grain-size distribution. In either case, the fact that both varieties of low-albedo material exhibit an aromatic hydrocarbon signature, and the expectation that aromatic hydrocarbons, specifically PAHs, are short-lived globally in the Iapetus radiation environment, strongly suggests that this material represents a recent and probably on-going deposit.

Our Gaussian decomposition of the organic band region suggests the presence of molecular bands in addition to those noted above, specifically bands attributable to cycloalkanes, olefinic compounds, CH_3OH, and N-substituted PAHs, as well as possible H_n-PAHs. Interpreting the Gaussian band fitting with two aromatic band components and the asymmetric CH_2 and CH_3 bands taken into account, we find the ratio of aromatic CH to aliphatic $CH_2 + CH_3$ functional groups for both the leading and trailing hemispheres of Iapetus is ~10. The ratio CH_2/CH_3 in the same two asymmetric bands is 4.0 on the leading hemisphere and 3.0 on the trailing; both values are higher than those found in interstellar dust and other Solar System materials and the difference between the two hemispheres may be statistically significant. Together, these two measures of the organic content of the Iapetus material distinguish this body (and Hyperion and Phoebe) apart from nearly all other Solar System materials that have been measured in space and in the laboratory to date.

Grains presently coating the leading hemisphere of Iapetus appear to carry the compositional signature of native Phoebe material and that material presents a combination of hydrocarbons not detected on other Solar System bodies. It must be noted, however, that there are very few observations of Solar System bodies in the relevant wavelength region (3.0–3.8 μm) with sufficient signal precision to detect the weak hydrocarbon bands, which in some cases are nearly obscured by H_2O ice spectral features. The acquisition of data of sufficient quality to explore whether these hydrocarbons are widespread, or if they are unique to Phoebe, is an appealing goal as observational capabilities improve. Such data will also bear upon Phoebe's compositional relationship to bodies remaining in the transneptunian region where it is thought to have originated (Johnson and Lunine 2005).

Acknowledgments

We thank Drs. Hiroshi Imanaka, L.J. Allamandola, M.P. Bernstein, A.G.G.M. Tielens, Diane H. Wooden, and especially S.A. Sandford for helpful conversations as this work progressed. This work is supported in part by the NASA Cassini project, the VIMS team, and Cassini Data Analysis program (R. Clark and C.M. Dalle Ore, Principal Investigators).

Appendix A

A.1. Models of Iapetus

Hapke scattering models for the best fits to the spectra of Iapetus leading and Iapetus trailing in the interval 2.7–4.0 μm were calculated in an iterative procedure in the way that was used by Clark et al. (2012, e.g., Fig. 3c). The entire spectrum from 1.0 to 4.0 μm was modeled by varying the abundances and grain sizes of the components, which are hematite (with embedded CO_2), nanophase free iron, and H_2O ice at 110 K. The optical constants for H_2O ice are those of Mastrapa et al. (2009) with some modifications in the 3.0–3.8 μm region to bring them into conformity with laboratory spectra of high precision at temperatures relevant to the Saturn satellites. The principal criteria for fitting a model to the data are matching (1) the very weak Fresnel peak at 3.12 μm, (2) the depth and shape of the broad 3-μm absorption, (3) the albedo level in the region 2.97–4.0 μm, and (4) the strength of the H_2O ice bands at 1.55 and 2.0 μm. These criteria can be met with the materials noted, and the band shapes and albedo levels require that very fine grains (micrometer and sub-micrometer) of both H_2O ice and neutral iron be employed. The Hapke scattering code was modified (see also Clark et al., 2012) to accommodate the very small particles, which are normally excluded from the Hapke formulation.

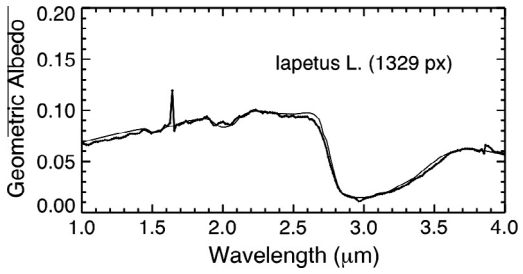

Fig. A1. Average spectrum of the selected spatial pixels on the leading hemisphere of Iapetus and the computed reflectance model. Note that the spike at 1.65 μm and the small discrepancies at 2.98 and 3.86 μm arise from filter junctions in the VIMS instrument and are not modeled here. Clark et al. (2012) have pointed out that the dip in the spectrum at 2.98 μm may indicate the presence of NH_3 on Iapetus, but the coincidence of the filter junction with the ammonia band leaves the question open. NH_3 was not included in the models shown in this figure.

Table A1
Leading hemisphere (Fig. 3B).

Central wavelength (μm)	Derived FWHM (cm^{-1})	Optical depth, τ	Gaussian identified in Fig. 3B
3.226	30.6	0.046	a
3.260	30.1	0.054	b
3.280	29.9	0.029	c
3.306	30.1	0.039	d
3.381	30.2	0.033	e
3.418	30.7	0.068	f
3.453	30.3	0.058	g
3.483	30.2	0.054	h
3.509	30.2	0.053	i
3.537	30.1	0.056	j
3.566	30.6	0.043	k

Our best-fit model for the two Iapetus spectra is shown for the full spectral range of 1.0–4.0 μm in Fig. A1; Fig. 1 in the present paper shows enlarged versions of the 2.7–4.0-μm region of the full spectra. The model for the Iapetus leading hemisphere fits the data for both hemispheres well, and is used for both leading and trailing spectra because the region of the organic bands, which is the central point of the present paper, is well matched and thereby provides the basis for the removal of the background absorption to reveal the aromatic and aliphatic absorption bands (3.1–3.6 μm). We have, however, made a small vertical offset of the model for extraction of the organic bands from the trailing hemisphere spectrum to ensure that the intersections of the model and the data occur at the same wavelengths as they do with the leading hemisphere spectrum. The net effect of using the same model for both hemispheres is to introduce a small arbitrary offset in model/data that also affects the amplitude of the extracted spectra. Because we are working with ratios of spectral features within each spectrum separately, the offset does not affect the final results presented here.

A.2. Gaussian fits to full band profiles

These tables give the Gaussian band fitting parameters corresponding to Fig. 3B and D.

A.3. Steps taken in data processing in this work

This is the sequence of steps taken to extract the average spectra of the low-albedo material on the leading and trailing hemispheres of Iapetus that are analyzed in this paper.

Table A2
Trailing hemisphere (Fig. 3D).

Central wavelength (μm)	Derived FWHM (cm^{-1})	Optical depth, τ	Gaussian identified in Fig. 3D
3.226	30.8	0.066	a
3.260	30.3	0.077	b
3.280	30.0	0.055	c
3.309	30.7	0.076	d
3.381	30.8	0.064	e
3.418	31.5	0.105	f
3.453	30.6	0.088	g
3.483	30.4	0.074	h
3.509	30.3	0.068	i
3.537	30.1	0.062	j
3.566	30.6	0.058	k

1. The mosaic of VIMS hyperspectral data cubes for Iapetus assembled by Pinilla-Alonso et al. (2011) is the basic data set used in this investigation. The data were acquired on September 10, 2007, on orbit 49 of the Cassini spacecraft.
2. A clustering algorithm defined on the spectral interval 2.9–3.8 μm was run on the spectra for each pixel in the entire mosaic to select the water–ice-poor, low-albedo pixels over the surface of Iapetus.
3. Each individual spectrum of the cluster representing the geographic regions with the lowest albedo and minimum presence of H_2O ice absorption bands was divided by a polynomial spline with the following wavelengths: 3.007, 3.090, 3.190, 3.200, 3.345, 3.529, 3.530, 3.612, 3.640, and 3.659 μm. This gave a first-order correction to the data to flatten the continuum of each spectrum.
4. The clustering software was run on the continuum-corrected spectra, yielding two distinct clusters that naturally separated pixels from the leading and trailing hemispheres. The average spectra of the leading and trailing hemispheres were calculated from the cluster results.
5. A model was fit to each of the two average spectra in several iterative steps, as described in Appendix A.1 (Fig. 1), and the ratio of the model to the average spectrum for each hemisphere was calculated (Fig. 2).
6. A four-point spline was fit to the high points in the ratio spectrum in step 5 to level the continuum thus defined.
7. Gaussian fits to the two model-removed spectra were calculated, as described in the text and shown in Fig. 3 and tabulated in Tables 3, 4, A1 and A2.

References

Allamandola, L.J., 2011. PAHS and astrobiology. EAS Publ. Ser. 46, 305–317. http://dx.doi.org/10.1051/eas/1146032.
Barucci, M.A., Merlin, F., Dotto, E., Doressoundiram, A., de Bergh, C., 2006. TNO surface ices. Observations of the TNO 55638 (2002 VE_{95}). Astron. Astrophys. 455, 725–730.
Bauschlicher Jr., C.W., Peeters, E., Allamandola, L.J., 2008. The infrared spectra of very large, compact, highly symmetric, polycyclic aromatic hydrocarbons (PAHs). Astrophys. J. 678, 316–327.
Bauschlicher Jr., C.W., Peeters, E., Allamandola, L.J., 2009. The infrared spectra of very large irregular polycyclic aromatic hydrocarbons (PAHs): Observational probes of astronomical PAH geometry, size, and charge. Astrophys. J. 697, 311–327.
Bellamy, L.J., 1975. The Infra-red Spectra of Complex Molecules, third ed. Chapman and Hall, London, 433pp.
Bernstein, M.P., Sandford, S.A., Allamandola, L.J., 1996. Hydrogenated polycyclic aromatic hydrocarbons and the 2940 and 2850 wavenumber (3.40 and 3.51 μm) infrared emission features. Astrophys. J. 472, L127–L130.
Bockelée-Morvan, D., Brooke, T.Y., Crovisier, J., 1995. On the origin of the 3.2- to 3.6-μm emission features in comets. Icarus 116, 18–39.
Bottke, W.F., Nesvorný, D., Vokrouhlický, D., Morbidelli, A., 2010. The irregular satellites: The most collisionally evolved populations in the Solar System. Astron. J. 139, 994–1014.

Brown, R.H. et al., 2004. The Cassini Visual and Infrared Mapping Spectrometer investigation. Space Sci. Rev. 115 (Cassini Issue), 111–168.
Brown, R.H. et al., 2006. Observations in the Saturn system during approach and orbital insertion, with Cassini's Visual and Infrared Mapping Spectrometer (VIMS). Astron. Astrophys. 446, 707–716.
Carrez, P. et al., 2002. Low-energy helium ion irradiation-induced amorphization and chemical changes in olivine: Insights for silicate dust evolution in the interstellar medium. Meteorit. Planet. Sci. 37, 1599–1614.
Clark, R.N. et al., 2005. Compositional mapping of Saturn's moon phoebe with imaging spectroscopy. Nature 435, 66–69.
Clark, R.N., Brown, R.H., Jaumann, R., Cruikshank, D.P., Buratti, B., Baines, K.H., Nelson, R.M., Nicholson, P.D., Moore, J.M., Curchin, J.M., Hoefen, T., Stephan, K., 2008. Compositional mapping of Saturn's satellite Dione with Cassini VIMS and the implications of dark material in the Saturn system. Icarus 193, 372–386.
Clark, R.N., Curchin, J.M., Hoefen, T.M., Swayze, G.A., 2009. Reflectance spectroscopy of organic compounds I: Alkanes. J. Geophys. Res. 114, E03001. http://dx.doi.org/10.1029/2008JE003150.
Clark, R.N., Cruikshank, D.P., Jaumann, R., Brown, R.H., Stephan, K., Dalle Ore, C.M., Livio, K.E., Pearson, N., Curchin, J.M., Hoefen, T.M., Buratti, B.J., Filacchione, G., Baines, K.H., Nicholson, P.D., 2012. The surface composition of Iapetus: Mapping results from Cassini VIMS. Icarus 218, 831–860.
Clemett, S.J. et al., 1998. Observations of indigenous polycyclic aromatic hydrocarbons in "giant" carbonaceous Antarctic micrometeorites. Orig. Life Evol. Biosp. 28, 425–448.
Clemett, S.J., Sandford, S.A., Nakamura-Messenger, K., Horz, F., McKay, D.S., 2010. Complex aromatic hydrocarbons in *Stardust* samples collected from Comet 81P/Wild2. Meteorit. Planet. Sci. 45, 701–722.
Colangeli, L., Mennella, V., Bussoletti, E., 1992. Temperature dependence of infrared bands produced by polycyclic aromatic hydrocarbons. Astrophys. J. 385, 577–584.
Coradini, A., Tosi, F., Gavrichin, A.I., Capaccioni, F., Cerroni, P., Filacchione, G., Adriani, A., Brown, R.H., Bellucci, G., Formisano, V., D'Aversa, E., Lunine, J.I., Baines, K.H., Bibring, J.-P., Buratti, B.J., Clark, R.N., Cruikshank, D.P., Combes, M., Drossart, P., Jaumann, R., Langevin, Y., Matson, D.L., McCord, T.B., Mennella, V., Nelson, R.M., Nicholson, P.D., Sicardy, B., Sotin, C., Hedman, M.M., Hansen, G.B., Hibbitts, C.A., Showalter, M., Griffith, C., Strazzulla, G., 2008. Identification of spectral units on Phoebe. Icarus 193, 233–251.
Corrsin, L., Fax, B.J., Lord, R.C., 1953. The vibrational spectra of pyridine and pyridine-d_5. J. Chem. Phys. 21, 1170–1177.
Cruikshank, D.P., Bell, J.F., Gaffey, M.J., Brown, R.H., Howell, R., Beerman, C., Rognstad, M., 1983. The dark side of Iapetus. Icarus 53, 90–104.
Cruikshank, D.P., Roush, T.L., Bartholomew, M.J., Geballe, T.R., Pendleton, Y.J., White, S.M., Bell III, J.F., Davies, J.K., Owen, T.C., de Bergh, C., Tholen, D.J., Bernstein, M.P., Brown, R.H., Tryka, K.A., Dalle Ore, C.M., 1998. The composition of Centaur 5145 Pholus. Icarus 135, 389–407.
Cruikshank, D.P., Dalton, J.B., Dalle Ore, C., Bauer, J., Stephan, K., Cassini VIMS and UVS Teams, et al., 2007. Surface composition of Hyperion. Nature 448, 54–56.
Cruikshank, D.P., Wegryn, E., Dalle Ore, C.M., Brown, R.H., Baines, K.H., Bibring, J.-P., Buratti, B.J., Clark, R.N., McCord, T.B., Nicholson, P.D., Pendleton, Y.J., Owen, T.C., Filacchione, G., Coradini, A., Cerroni, P., Capaccioni, F., Jaumann, R., Nelson, R.M., Baines, K.H., Sotin, C., Bellucci, G., Combes, M., Langevin, Y., Sicardy, B., Matson, D.L., Formisano, V., Drossart, P., Mennella, V., 2008. Hydrocarbons on Saturn's satellites Iapetus and Phoebe. Icarus 193, 334–343.
Dalle Ore, C.M., Cruikshank, D.P., Clark, R.N., 2012. Infrared spectroscopic characterization of the low-albedo materials on Iapetus. Icarus 221, 735–743.
Dalton, J.B., Cruikshank, D.P., Clark, R.N., 2012. Compositional analysis of Hyperion with Cassini VIMS. Icarus 220, 752–776.
Dartois, E., Marco, O., Muñoz-Caro, G.M., Brooks, K., Deboffle, D., d'Hendecourt, L., 2004a. Organic matter in Seyfert 2 nuclei: Comparison with our galactic center lines of sight. Astron. Astrophys. 423, 549–558.
Dartois, E., Muñoz-Caro, G.M., Deboffle, D., d'Hendecourt, L., 2004b. Diffuse interstellar medium organic polymers: Photoproduction of the 3.4, 6.85, and 7.25 μm features. Astron. Astrophys. 423, L33–L36.
Denk, T. et al., 2010. Iapetus: Unique surface properties and a global color dichotomy from Cassini imaging. Science 327, 435–439.
d'Hendecourt, L., Allamandola, L.J., 1986. Time dependent chemistry in dense molecular clouds. III. Infrared band cross sections of molecules in the solid state at 10 K. Astron. Astrophys. Suppl. 64, 453–467.
Filacchione, G., Capaccioni, F., Ciarniello, M., Clark, R.N., Cuzzi, J.N., Nicholson, P.D., Cruikshank, D.P., Hedman, M.M., Buratti, B.J., Lunine, J.I., Soderblom, L.A., Tosi, F., Cerroni, P., Brown, R.H., McCord, T.B., Jaumann, R., Stephan, K., Baines, K.H., Flamini, E., 2012. Saturn's icy satellites and rings investigated by Cassini-VIMS: III – Radial compositional variability. Icarus 220, 1064–1096.
Flynn, G.J., Keller, L.P., Jacobsen, C., Wirick, S., 2004. An assessment of the amount and types of organic matter contributed to the Earth by interplanetary dust. Adv. Space Res. 33, 57–66.
Gudipati, M.S., Yang, R., 2012. In situ probing of radiation-induced processing of organics in astrophysical ice analogs—Novel laser desorption laser ionization time-of-flight mass spectroscopic studies. Astrophys. J. 756, L24–L28.
Hand, K.P., Carlson, R.W., 2012. Laboratory spectroscopic analyses of electron-irradiated alkanes and alkenes in Solar System ices. J. Geophys. Res. 117, E03008.
Hudgins, D.M., Sandford, S.A., 1998. Infrared spectroscopy of matrix isolated polycyclic aromatic hydrocarbons. 1. PAHs containing two to four rings. J. Phys. Chem. A 102, 329–343.
Jarvis, K.S., Vilas, F., Larson, S.M., Gaffey, M.J., 2000. Are Hyperion and Phoebe linked to Iapetus? Icarus 146, 125–132.
Johnson, R.E., 1989. Effect of irradiation on the surface of Pluto. Geophys. Res. Lett. 16, 1233–1236.
Johnson, T.V., Lunine, J.I., 2005. Saturn's moon Phoebe as a captured body from the outer Solar System. Nature 435, 69–71.
Mastrapa, R.M., Sandford, S.A., Roush, T.L., Cruikshank, D.P., Dalle Ore, C.M., 2009. Optical constants of amorphous and crystalline H_2O ice: 2.5–22 μm (4000–455 cm^{-1}). Astrophys. J. 701, 1347–1356.
Matrajt, G., Muñoz Caro, G.M., Dartois, E., d'Hendecourt, L., Deboffle, D., Borg, J., 2005. FTIR analysis of the organics in IDPs: Comparison with the IR spectra of the diffuse interstellar medium. Astron. Astrophys. 433, 979–995.
Matrajt, G., Flynn, G., Brownlee, D., Joswiak, D., Bajt, S., 2013. The origin of the 3.4-μm feature in Wild 2, cometary particles and in ultracarbonaceous interplanetary dust particles. Astrophys. J. 765, 145–163.
Mumma, M.J., Charnley, S.B., 2011. The chemical composition of comets – Emerging taxonomies and natal heritage. Annu. Rev. Astron. Astrophys. 49, 471–524.
Pendleton, Y.J., 2004. Hydrocarbons in meteorites, the Milky Way, and other galaxies. In: Witt, A.N., Clayton, G.C., Draine, B.T. (Eds.), Astrophysics of Dust. ASP Conf. Series 309. pp. 573–587.
Pendleton, Y.J., Allamandola, L.J., 2002. The organic refractory material in the diffuse interstellar medium: Mid-infrared spectroscopic constraints. Astrophys. J. Suppl. 138, 75–98.
Pendleton, Y.J., Sandford, S.A., Allamandola, L.J., Tielens, A.G.G.M., Sellgren, K., 1994. Near-infrared absorption spectroscopy of interstellar hydrocarbon grains. Astrophys. J. 437, 683–696.
Pinilla-Alonso, N., Roush, T.L., Marzo, G.A., Cruikshank, D.P., Dalle Ore, C.M., 2011. Iapetus surface variability revealed from statistical clustering of a VIMS mosaic: The distribution of CO_2. Icarus 215, 75–82.
Ricca, A., Bauschlicher Jr., C.W., Boersma, C., Tielens, A.G.G.M., Allamandola, L.J., 2012. The infrared spectroscopy of compact polycyclic aromatic hydrocarbons containing up to 384 carbons. Astrophys. J. 754, 75 (22pp.).
Ristein, J., Stief, R.T., Ley, L., Beyer, W., 1998. A comparative analysis of a-C:H by infrared spectroscopy and mass selected thermal effusion. J. Appl. Phys. 84, 3836–3847.
Sandford, S.A., 2008. Terrestrial analysis of the organic component of comet dust. Annu. Rev. Anal. Chem. 1, 549–578.
Sandford, S.A., Allamandola, L.J., Tielens, A.G.G.M., Sellgren, K., Tapia, M., Pendleton, Y., 1991. The interstellar C—H stretching band near 3.4 μm: Constraints on the composition of organic material in the diffuse interstellar medium. Astrophys. J. 371, 607–620.
Sandford, S.A., Aleon, J., Alexander, C.M.O'D., 2006. Organics captured from Comet 81P/Wild 2 by the *Stardust* spacecraft. Science 314, 1720–1724.
Sandford, S.A., Bernstein, M.P., Materese, C.K., 2013. The infrared spectra of polycyclic aromatic hydrocarbons with excess peripheral H atoms (H_n-PAHs) and their relation to the 3.4 and 6.9 μm PAH emission features. Astrophys. J. Suppl. 205, 8 (30pp.).
Silverstein, R.M., Bassler, G.C., Morrill, T.C., 1981. Spectrometric Identification of Organic Compounds, fourth ed. Wiley, New York, 442pp.
Sobkowiak, M., Painter, P., 1992. Determination of the aliphatic and aromatic CH contents of coals by FTIR: Studies of coal extracts. Fuel 71, 1105–1125.
Strazzulla, G., 1986. Organic material from Phoebe to Iapetus. Icarus 66, 397–400.
Strazzulla, G., Cooper, J.F., Christian, E.R., Johnson, R.E., 2003. Ion irradiation of TNOs: From the fluxes measured in space to the laboratory experiments. CR Phys. 4, 791–801.
Sunshine, J.M., Pieters, C.M., 1993. Estimating modal abundances from the spectra of natural and laboratory pyroxene mixtures using the modified Gaussian model. J. Geophys. Res. 98, 9075–9087.
Sunshine, J.M., Pieters, C.M., Pratt, S.F., 1989. Mathematical deconvolution of mineral absorption bands. Lunar Planet. Sci. XX. Abstract 1087.
Tamayo, D., Burns, J.A., Hamilton, D.P., Hedman, M.M., 2011. Finding the trigger to Iapetus' odd global albedo pattern: Dynamics of dust from Saturn's irregular satellites. Icarus 215, 260–278.
Tosi, F., Turrini, D., Coradini, A., Filacchione, G., the VIMS Team, 2010. Probing the origin of the dark material on Iapetus. Mon. Not. R. Astron. Soc. 403, 1113–1130.
van Diedenhoven, B. et al., 2004. The profiles of the 3–12 μm polycyclic aromatic hydrocarbon features. Astrophys. J. 611, 928–939.
Verbiscer, A.J., Skrutskie, M.F., Hamilton, D.P., 2009. Saturn's largest ring. Nature 461, 1098–1100.
Wagner, D.R., Kim, H.S., Saykally, R.J., 2000. Perpherally hydrogenated neutral polycyclic aromatic hydrocarbons as carriers of the 3-μm interstellar infrared emission complex: Results from single-photon infrared emission spectroscopy. Astrophys. J. 545, 854–860.
Wexler, A.S., 1967. Integrated intensities of absorption bands in infrared spectroscopy. Appl. Spectrosc. Rev. 1, 29–98.
Wright, G.S., Bridger, A., Geballe, T.R., Pendleton, Y., 1996. Studies of NIR dust absorption features in the nuclei of active and IRAS galaxies. In: Block, D.L., Greenberg, J.M. (Eds.), New Extragalactic Perspectives in the New South Africa. Kluwer, Dordrecht, pp. 143–150.